Functional Materials Letters
Vol. 8, No. 4 (2015) 1550033 (5 pages)
© World Scientific Publishing Company
DOI: 10.1142/S1793604715500332

World Scientific
www.worldscientific.com

Reliable resistive switching and its tunability in La-doped $PbTiO_3 \backslash TiO_2$ composite bilayer

Ying Wang[*,†], Shaopeng Lin[†,‡], Xiaoyue Zhang[†,‡], Weiming Xiong[*,†],
Biao Wang[*,†,§,||] and Yue Zheng[*,†,¶,||]

*State Key Laboratory of Optoelectronic Materials and Technologies
School of Physics and Engineering
Sun Yat-sen University, Guangzhou 510275, P. R. China

†Micro & Nano Physics and Mechanics Research Laboratory
School of Physics and Engineering
Sun Yat-sen University, Guangzhou 510275, P. R. China

‡Sino-French Institute of Nuclear Engineering and Technology, Zhuhai Campus
Sun Yat-sen University, Zhuhai 519082, P. R. China
§wangbiao@mail.sysu.edu.cn
¶zhengy35@mail.sysu.edu.cn

www.spm.com.cn

Received 29 September 2014; Accepted 8 December 2014; Published 20 January 2015

Nanoscale La-doped $PbTiO_3$(PLT)$\backslash TiO_2$ (PLTT) composite structures have been fabricated. It shows that the structure presents reliable resistive switching (RS) behavior, and importantly, has great tunability on RS characteristics such as forming/set/reset voltages and resistance ratio by adjusting the PLT layer thickness. Particularly, the set voltage can be tuned at a large range from several volts to dozens of volts. Meanwhile, the set current keeps almost the same, indicating the RS is current dominating. The space-charge-limited current (SCLC) feature indicates that the localized traps are decisive for the RS. Our result sheds light on the prospects of composite structures for designing tunable RS devices.

Keywords: PLTT composite bilayer; resistive switching; tunable switching voltage; SCLC conduction.

Recently, resistive switching (RS) behaviors have attracted intense attentions due to the outstanding features such as nonvolatility and good scalability, which are promising in applications of both switches and resistance random access memory (RRAM) devices.[1–10] Various material systems have been reported for their RS behaviors, including metal binary oxides such as ZnO,[3] NiO[4] and TiO_2,[5] transition metal oxides (e.g., $Pb(Zr,Ti)O_3$,[1] $SrTiO_3$,[6] $BiFeO_3$[7,8] and $BiCoO_3$[9]), organic compounds,[10] and even SiO_2.[11] Attentions also have been paid on the mechanisms of RS behavior, with different possible theoretical models being proposed, such as conductive filament model,[6] Schottky barrier model[7] and charge trap-detrap model,[1] which are lately categorized into two types: Filament[2,3] and interface switching.[10]

In literature, many researchers have focused their studies on pursuing lower set-reset voltages and higher reliabilities, with some materials such as TiO_2 proved as promising candidates.[12,13] Despite the lacking of clear understanding, it has also been reported that multilayer integrating[14–16] or doping[11] can improve the performance of RS, such as reducing leakage current, improving electrical properties of films, as well as getting higher uniformity, better fatigue endurance and lower set-reset voltages. Nevertheless, more works are still required to gain a better control on RS behaviors. Particularly, for multilayer structures, few works have been reported in how the RS performance depends on structure. The RS characteristics (e.g., forming/set/reset voltages and resistance ratio) should be strong functions on the layer thickness, which is important for designing tunable RS devices, such as switches requiring various voltage levels.

In this paper, we report reliable RS behavior in nanoscale La-doped $PbTiO_3$(PLT)$\backslash TiO_2$ (PLTT) composite structures, and propose a flexible way to tune the RS behavior by adjusting the PLT layer thickness. It shows that the PLTT heterostructures exhibit significant tunability on the RS

||Corresponding authors.

behaviors such as forming/set/reset voltages and resistance ratio. The mechanism of the RS behavior is also analyzed.

La-doped $PbTiO_3$ (PLT: $Pb_{(1-x)}La_xTi_{1-x/4}O_3$, $x = 0.05$), TiO_2, and PLTT (PLT\$TiO_2$) multilayer composite thin films were prepared by chemical solution deposition (CSD) method on Pt\Ti\$SiO_2$\Si substrates.[17,18] To prepare PLT seeding layers, $(CH_3COO)_2Pb \cdot 3H_2O$, $La(NO_3)_3 \cdot nH_2O$, and titanium isopropoxide were utilized as starting materials, 2-methoxyethanol as solvent, and acetic acid as catalyst. Excess 5 mol% $(CH_3COO)_2Pb{\cdot}3H_2O$ was used to compensate the expected loss of volatile Pb during annealing process. The 0.4 mol/L PLT stoichiometric solution was spin-coated on the substrate at 3500 rpm for 25 s and prefired at 450°C for 5 min in air to remove volatile materials, which were repeated several times to fabricate three kinds of PLT films with desired thicknesses. Then the films were annealed at 700°C for an hour in air ambient. Similarly, for synthesis of TiO_2 thin films, Titanium isopropoxide was used as starting materials, and deionized water, anhydrous ethanol, acetic acid as solvent. The spin-coated 0.4 mol/L TiO_2 gel was prefired at 350°C for 5 min and annealed at 600°C for 1 h in air. To obtain the PLTT heterostructures, the previous three kinds of PLT thin films were used as seeding layers for the subsequent growth of TiO_2 films. Afterwards, Pt top electrodes with diameter of 0.5 mm were sputtered by dc magnetron sputtering on the films to form the Pt\PLTT\Pt structures shown in Fig. 1(a). Here to, five samples including Pt\$TiO_2$(385 nm)\Pt (S1), Pt\PLT(690 *nm*)\Au (S2), Pt\PLT(175 nm)\$TiO_2$\Pt (S3), Pt\PLT(370 nm)\$TiO_2$\Pt (S4) and Pt\PLT(690 nm)\$TiO_2$\Pt (S5) were obtained. Thicknesses of the layers were acquired from their cross-section images.

The crystallinity and phases of the grown films were analyzed in θ–2θ mode by a Rigaku (D-MAX 2200VPC) X-ray diffractometer (XRD) with CuKα radiation ($\lambda = 0.154$ nm) at 40 kV and 30 mA. The cross-section and morphology structure of the pristine films were confirmed by Quanta 400F scanning electron microscopy (SEM) and CSPM5500 scanning probe microscopy. Current-voltage (C–V) characteristics were measured by using a Keithley 4200 semiconductor characterization system (SCS) at room temperature in atmosphere, with the environment humidity of 25%.

The Pt/PLTT/Pt structure has been demonstrated in Fig. 1(a) and the SEM cross section image of the film was studied

www.spm.com.cn

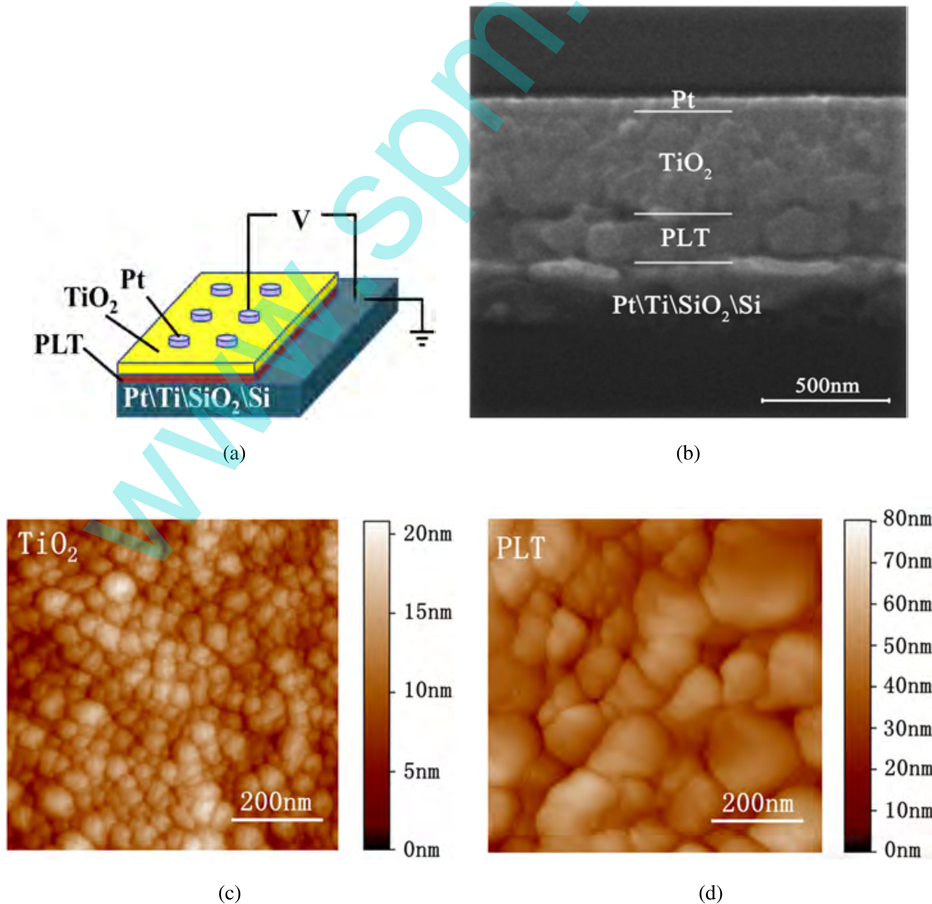

Fig. 1. The schematic diagram (a) and SEM cross-sectional image (b) of Pt\PLTT\Pt devices. Surface morphologies and grain sizes of TiO_2 (c) and PLT (d) thin films measured by AFM.

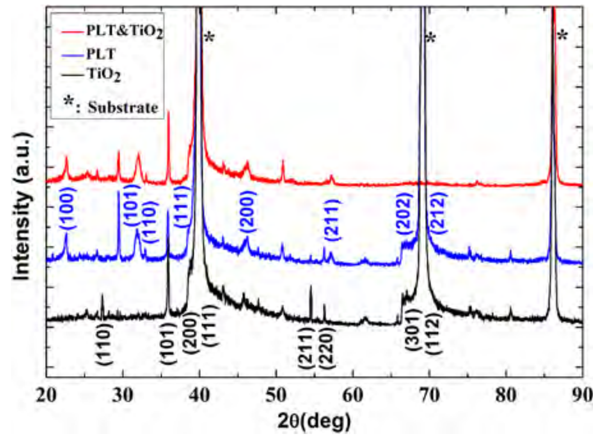

Fig. 2. XRD patterns of Pt\PLTT\Pt, Pt\PLT\Au, and Pt\TiO_2\Pt devices.

for acquiring the thickness of each layers. S3 is shown in Fig. 1(b) as an example with the thickness of Pt top electrode being 45 nm. Although the interface is slightly rough for TiO_2 on PLT seed layers (which is likely due to the interdiffusion caused by the high growth temperature), the PLTT structure was well grown on the substrates as expected.

The morphologies of TiO_2 and PLT thin films were studied by a scanning probe microscopy (SPM, CSPM5500). Both Figs. 1(c) and 1(d) show good crystallization of the TiO_2 and PLT thin films. The grain size of PLT (Fig. 1(d)) is much larger than TiO_2(Fig. 1(c)).

The XRD patterns of the films are shown in Fig. 2. The index Bragg reflections indicate that perovskite structure was formed in the PLT thin films and rutile structure formed in the TiO_2 thin films. Among the samples, no traces of impurity phases were found within the XRD detection limit. The XRD profiles of PLT thin film showed split reflection at $2\theta = 57.684^\circ$ and 45.233°, which indicated 5% lanthanum doping at Pb site.

The C–V characteristics of the prepared samples (S1, S2, S4) have been illustrated in Fig. 3. Figure 3(a) presents the typical behavior of bipolar RS (BRS) characteristics of the Pt\TiO_2\Pt capacitor as expected with a V_{Set} of 5.2 V and a compliance current of 10 mA for preventing the film from permanent breakdown. The inset shows the forming process for the first time with a compliance current of 1 mA at 17.2 V.

The conducting characteristics of PLT film was also studied (Fig. 3(b)). For simulating the asymmetric structure

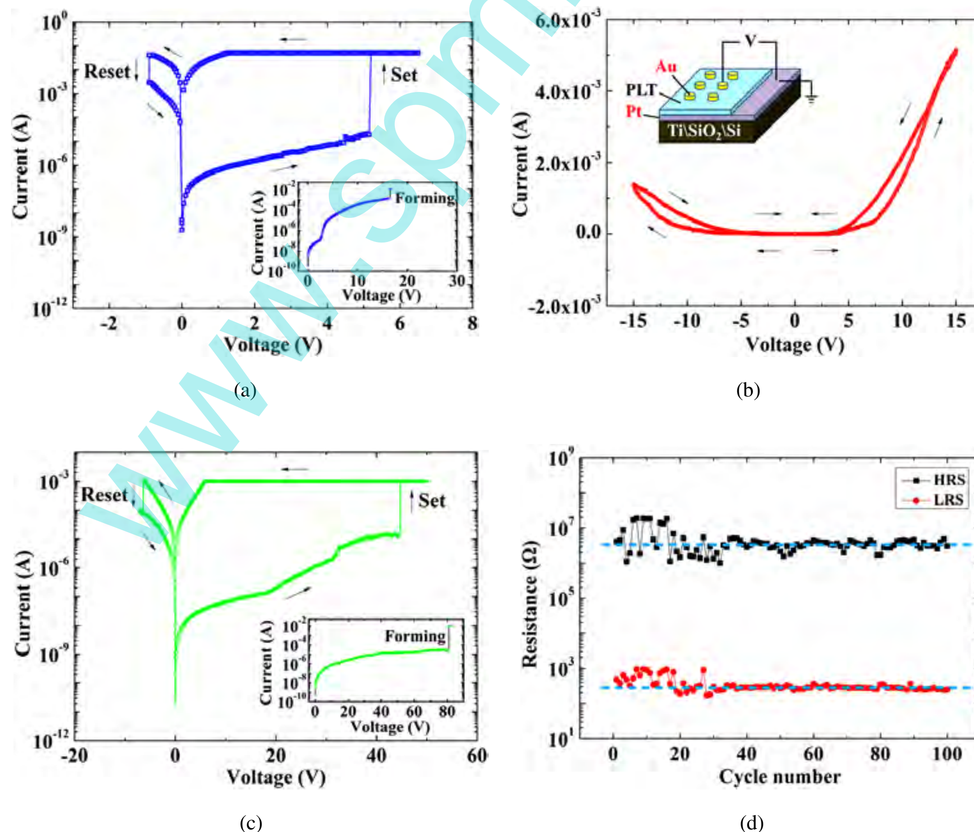

Fig. 3. The BRS current–voltage behaviors in Pt\TiO_2\Pt (a), Pt\PLT\Au (b), and Pt\PLTT\Pt heterostructure (c) with absolute values plotted in semi-log scale. The arrows indicate the direction of sweep voltage and the inset in right below corner shows the forming processes before BRS. The inset in the top left corner of (b) shows the sketch map of Pt\PLT\Au sample. (d) The resistance evolution of HRS and LRS in BRS process within 100 cycles plotted in semi-log scale, with the resistance ratio shown by blue fitting lines.

www.spm.com.cn

such as the TiO_2-PLT heterostructure, Au was chosen as the top electrode. Due to the comparatively wide bandgap of PLT, it is difficult for most electrons to jump from valence band into conduction band. When a certain "small" voltage is applied to the sample, as shown in Fig. 3(b), the energy is insufficient to impel numerous electrons jump into conduction band or activate abundant oxygen vacancies (OVs) migration in the films, which directly results in lack of conductive electrons and activated OVs. Therefore, the Pt\PLT\Au structure presents resistance-like characteristics in our experiments, with a high resistivity and low leakage current which blocks the emergence of RS behavior. As the magnitude of the applied voltage increases, the migration velocity of electrons and holes rises gradually and the current reaches the order of mA, which is in the range of compliance current for TiO_2, providing the possibility of RS behaviors in the substantial PLTT cells. It's worthy to mention that in the negative side, the impedance is much larger than that in the positive side because of the asymmetry of this structure.

By integrating TiO_2 and PLT thin film, it can be clearly seen from Fig. 3(c) that the PLTT heterostructure significantly regulates the RS characteristics of TiO_2. For S5, the forming voltage goes up to a tremendous value of 82 V as shown in the inset and V_{set} turns out to be about 45 V, which is very large and almost impossible to realize through simple change of TiO_2 thin films. The influence can be mainly divided into two kinds: polarization switching and impedance change. Because of the large leakage current in the PLT layer, electrical field in the film which should be large enough to switch the spontaneous polarization is too week, so the hysteresis loops in PLT layer cannot be successfully obtained. Thus the tuning function is mainly attributed to the impedance change. As we can see from Figs. 3(a) and 3(b), the impedance of the PLT layer is much larger than that of the TiO_2 layer. Another impedance (R_{hs}) caused by the heterostructure of the PLT and TiO_2 should also be taken into considerations. When the applied voltage on the Pt\PLTT\Pt cell rises from 0 V, most of it applies on the PLT layer following the Ohm's law. When the voltage on the PLT layer (V_{PLT}) increases, the impedance of the PLT layer decreases as shown in Fig. 3(b), resulting in rising current up to the range of mA. At the same time, the current is sufficient for the TiO_2 layer to take up resistance switching. Compliance current of 15 V is applied to prevent breakdown and probable RS in PLT layers which may lead more complex phenomena. RS in PLT cell will be studied in our following works. When a negative voltage applied on the PLTT cell under LRS, about 10 V is required to apply on the PLT layer to maintain the conduction current, so V_{reset} is also higher than that in S1. The set–reset processes have been reproduced and the resistance evolution of HRS and LRS of the PLTT cell is demonstrated in Fig. 3(d) with a readout voltage of 5 V. Although both the HRS and LRS exhibit some variation in the first thirty switching cycles, they become rather stable afterwards. As the light blue fitting lines show, the resistance ratio is almost four orders of magnitude, and shows no significant degradation of resistance within the whole 100 switching cycles, indicating stable and reproducible BRS characteristics of the PLTT cells.

Moreover, in order to explore the impact of PLT thickness in the PLTT cells, C–V characteristics of S3, S4 and S5 were also measured and illustrated in Fig. 4. Figure 4(a) shows the distribution of V_{set} for S3, S4 and S5 within 100 switching cycles, which is plotted in histograms. It can be clearly observed that V_{set} of the three samples all obey normal distribution, which are concentrated in relatively narrow distribution intervals of 9–11 V, 25–27 V and 43–45 V, respectively. To be more visualized, three C–V switching circles in each concentrated interval of the three samples have been picked out and shown in Fig. 4(b). As the thickness of PLT layer increases, V_{set} and V_{reset} become larger and larger. Especially the V_{set}, shows more sensitive to the change of thickness in PLT layer, strongly demonstrating the tuning function of PLT layer. Meanwhile, the set currents keep almost the same, demonstrating the RS is current dominating.

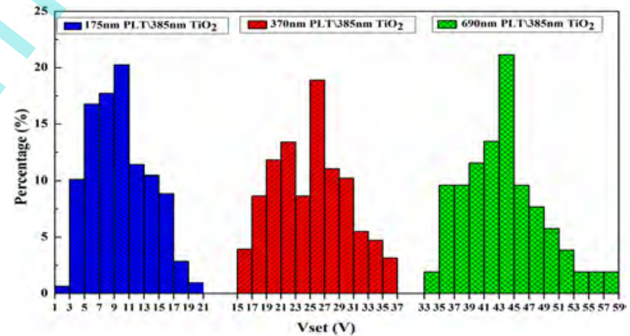

(a)

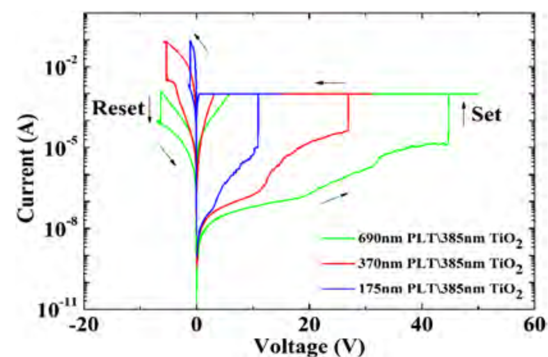

(b)

Fig. 4. (a) V_{set} distribution of the PLTT composite bilayers with different PLT layer thicknesses in 100 switching cycles. (b) The typical BRS current–voltage behaviors of the PLTT composite bilayers with different PLT layer thicknesses.

www.spm.com.cn

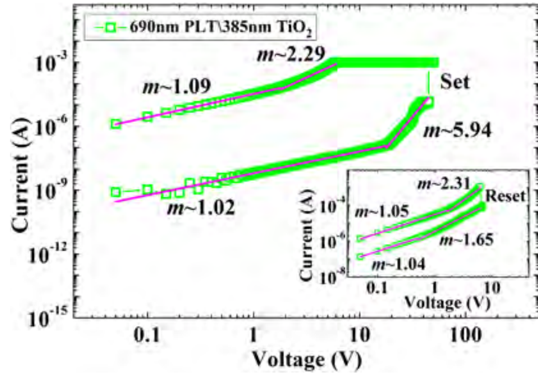

Fig. 5. The BRS current–voltage curves with both positive bias range and negative bias range (the inset in the bottom right corner) of S5 replotted on a log–log scale.

In addition, the HRS–LRS ratios also have been tuned as the change of PLT-layer-thickness, among which S3 shows improved RS ratio of 10^5. Importantly, the heterostructure of PLT and TiO_2 and the interface of the PLT sub layers (spin-coating layer by layer), which can generate barriers blocking the migration of the carriers, should be in relevance with the tuning behaviors.

To further analyze the BRS characteristics, the C–V curves of S5 in Fig. 4(b) have been replotted on a logarithmic scale for the sake of elucidating current conduction mechanism of the samples, shown in Fig. 5.

From the linear fitting results with pink lines, the slopes both in set and reset processes are similarly close to "1" in low voltage region, while obviously greater than "1" in relatively high voltage region. The results can be explained by the typical SCLC theory.[19,20] According to the SCLC conduction mechanism, in low voltage region, the concentration of injected carriers is lower than the thermal equilibrium carrier concentration, resulting in the current behavior showing Ohmic conduction property, where current linear to the voltage $(I \propto V^m, m \approx 1)$. As the voltage increases large enough to make the density of injected carriers greater than the equilibrium number of carriers, the Ohmic conduction transitions to the trap-controlled conduction $(I \propto V^m, m > 1)$, leading to the larger slope values in high voltage region. Since SCLC conduction mechanism is controlled by the localized traps of thin film, it is believed to be of great relevance to the RS behavior of the PLTT cells. Although metal/oxide Schottky junction in Pt/TiO_2 or Pt/PLT interface can have contribution in the device RS behavior,[21] the influence from oxygen vacancies or other defects should be dominant in the whole RS process when the tests are carried out in atmospheric environment according to previous studies.[5,15,22–24]

In summary, Pt\PLTT\Pt composite bilayer has been fabricated by CSD methods. C–V studies show that the structure presents reliable RS behavior and significant tunability for RS characteristics, such as set/reset/forming voltages and resistance ratio. By varying the thickness of PLT layer, the V_{set} can be adjusted at a large range from several to dozens of volts. In addition, the similar set currents demonstrate that the RS is current dominating. Based on current conduction analysis, trap-limited SCLC conduction mechanism is considered to be dominant in the whole RS process. The results will be advantageous for designing flexibly tunable switching elements.

Acknowledgments

The project was supported by NSFC (Nos. 51172291, 11232015, 11302268, 11402312), FRFCU, NCET, RFDPHE, FYTF and GDNSFDYS.

www.spm.com.cn

References

1. J. Choi *et al.*, *Appl. Phys. Lett.* **96**, 262113 (2010).
2. R. Waser and M. Aono, *Nat. Mater.* **6**, 833 (2007).
3. D. Xu *et al.*, *J. Alloy. Compd* **584**, 269 (2014).
4. D. Ielmini *et al.*, *Nanotechnology* **22**, 254022 (2011).
5. Y. H. Do *et al.*, *Appl. Phys. Lett.* **95**, 093507 (2009).
6. R. Muenstermann *et al.*, *J. Appl. Phys.* **108**, 124504 (2010).
7. A. Q. Jiang *et al.*, *Adv. Mater.* **23**, 1277 (2011).
8. J. M. Luo *et al.*, *Appl. Phys. Lett.* **101**, 062902 (2012).
9. B. Sun *et al.*, *Funct. Mater. Lett.* **8**, 1550001 (2014).
10. J. C. Scott and L. D. Bozano, *Adv. Mater.* **19**, 1452 (2007).
11. C. Schindler *et al.*, *Electron Devices, IEEE Trans.* **54**, 2762 (2007).
12. K. M. Kim *et al.*, *Nanotechnology* **22**, 254002 (2011).
13. D. S. Jeong *et al.*, *Rep. Prog. Phys.* **75**, 076502 (2012).
14. T. Fujii *et al.*, *Appl. Phys. Lett.* **86**, 012107 (2005).
15. W. J. Ma *et al.*, *Appl. Phys. Lett.* **103**, 262903 (2013).
16. Z. Wen *et al.*, *Nat. Mater.* **12**, 617 (2013).
17. J. Koo *et al.*, *J. Sol-Gel Sci. Techn.* **13**, 869 (1998).
18. W. Di *et al.*, *Thin Solid Films* **322**, 323 (1998).
19. D. R. Lamb, *Electrical Conduction Mechanisms in Thin Insulating Films* (Methuen, London, 1967).
20. J. F. Scott *et al.*, *J. Appl. Phys.* **70**, 382 (1991).
21. H. Lee *et al.*, *ACS Appl. Mater. Interfaces* **5**, 11668 (2013).
22. G. Tang *et al.*, *Nanoscale* **5**, 422 (2013).
23. Zheng *et al.*, *Appl. Phys. Lett.* **89**, 062904 (2006).
24. Zheng *et al.*, *Journal of the Mechanics and Physics of Solids* **55**, 1661 (2007).